Quantification and Characterization of P-Glycoprotein−Substrate Interactions

Ewa Gatlik-Landwojtowicz, Päivi Äänismaa, and Anna Seelig*

Biophysical Chemistry, Biozentrum, University of Basel, Klingelbergstrasse 70, CH-4056, Basel, Switzerland

Received July 15, 2005; Revised Manuscript Received November 29, 2005

ABSTRACT: It is generally accepted that P-glycoprotein binds its substrates in the lipid phase of the membrane. Quantification and characterization of the lipid-transporter binding step are, however, still a matter of debate. We therefore selected 15 structurally diverse drugs and measured the binding constants from water to the activating (inhibitory) binding region of P-glycoprotein, $K_{tw(1)}$ ($K_{tw(2)}$), as well as the lipid−water partition coefficients, K_{lw}. The former were obtained by measuring the concentrations of half-maximum activation (inhibition), K_1 (K_2), in living NIH-MDR-G185 mouse embryo fibroblasts using a Cytosensor microphysiometer, and the latter were derived from surface activity measurements. This allowed determination of the membrane concentration of drugs at half-maximum P-glycoprotein activation ($C_{b(1)}$ = (0.02 to 67) mmol/L lipid), which is much higher than the corresponding aqueous concentration (K_1 = (0.02 to 376) μM). Moreover we determined the free energy of drug binding from water to the activating binding region of the transporter ($\Delta G°_{tw(1)}$ = (−30 to −54) kJ/mol), the free energy of drug partitioning into the lipid membrane ($\Delta G°_{lw}$ = (−23 to −34) kJ/mol), and, as the difference of the two, the free energy of drug binding from the lipid membrane to the activating binding region of the transporter ($\Delta G°_{tl(1)}$ = (−7 to −27) kJ/mol). For the compounds tested $\Delta G°_{tl(1)}$ was less negative than $\Delta G°_{lw}$ but varied more strongly. The free energies of substrate binding to the transporter within the lipid phase, $\Delta G°_{tl(1)}$, are consistent with a modular binding concept, where the energetically most efficient binding module comprises two hydrogen bond acceptor groups.

Various lines of evidence indicate that the P-glycoprotein-ATPase, Pgp[1] (ABCB1), binds its substrates within the plasma membrane (*1*, *2*) and, more precisely, within the cytosolic lipid leaflet of the plasma membrane (*3*−*7*) (for review see ref *8*). Exogenous substrates such as drugs and toxins are thus caught by Pgp *after* partitioning into the plasma membrane but *before* reaching the cytosol and are then exported or flipped at the expense of ATP hydrolysis (*3*, *4*, *9*).

The environment from which substrates bind to the transporter is decisive for the type of binding interactions (*10*, *11*). Little is known on the role of the lipid membrane for substrate−transporter interactions since most well-investigated transporters bind their substrates from the aqueous phase (e.g. fucose transporter (*12*)). To investigate the relationship between lipid partitioning and drug binding Romsicki and Sharom (*13*) reconstituted Pgp into various well-defined lipid bilayers and measured the transporter dissociation constants, K_d (i.e. the release of the drug from Pgp into the aqueous phase), as well as the lipid−water partition coefficients, P_{lw}. For the three drugs investigated, the binding affinity to Pgp from the aqueous phase increased in parallel to the lipid−water partition coefficient, suggesting that the concentration of the drug in the membrane is important for the interaction with the transporter (*13*). A linear correlation between binding affinity to Pgp and membrane partitioning (estimated from the octanol−water partition coefficient, log P_{ow}) was also observed for propafenone analogues (*6*). However, for structurally more diverse drugs no correlation between binding affinity to Pgp and membrane affinity (log P_{ow}) was observed. Instead, an approximately linear dependence of the binding affinity to Pgp on the van der Waals surface area of drugs was noticed (*14*). For the same drugs, a linear correlation between drug affinity to Pgp and the logarithm of the air−water partition coefficient, log K_{aw}, was demonstrated (*15*), suggesting that both the lipid−water partition coefficient, K_{lw}, and the cross-sectional area, A_D, of a given drug molecule play a role for drug−Pgp interactions (*11*).

The question as to how Pgp accommodates molecules of different size is still a matter of debate. It has been suggested that Pgp has at least two substrate binding sites (*1*, *13*, *16*). Our kinetic data (*17*, *18*) could be well fitted with a model (*14*) that assumes two binding sites, one for activation and one for inhibition. Evidence for three (*19*) and even four binding sites has also been reported (*20*). As an alternative to specific binding sites, broader binding regions have been proposed (*21*). The concept of binding regions is consistent with a search for possible drug interaction sites in the

* Corresponding author. Phone: +41-61-267-22-06. Fax: +41-61-267-21-89. E-mail: Anna.Seelig@unibas.ch.

[1] Abbreviations: DMPC, 1,2-dimyristoyl-*sn*-glycero-3-phosphatidylcholine; ECAR, extracellular acidification rate; K_1 (K_2), aqueous substrate concentration at half-maximum Pgp activation (inhibition); K_{aw}, air−water partition coefficient; K_{lw}, lipid−water partition coefficient; $K_{tl(1)}$ ($K_{tl(2)}$), binding constant of the drug from the lipid membrane to the activating (inhibitory) binding region of the transporter; $K_{tw(1)}$ ($K_{tw(2)}$), binding constant of the drug from water to the activating (inhibitory) binding region of the transporter; MDR, multidrug resistance; Pgp, P-glycoprotein-ATPase (MDR1, ABCB1); POPC, 1-palmitoyl-2-oleoyl-*sn*-glycero-3-phosphatidylcholine; π_M, lateral membrane packing density; V_1 (V_2), maximum (minimum) transporter activity.

10.1021/bi051380+ CCC: $33.50
Published on Web 02/07/2006

predicted transmembrane sequences of Pgp (*22*). The latter investigation revealed a high density of amino acids with hydrogen bond donor side chains in the transmembrane sequences of Pgp which could interact with characteristic hydrogen bond acceptor patterns present in *all* Pgp substrates (*10*, *23*, *24*). Moreover, clusters of phenyl residues were observed which could interact either with π-electron systems ($\pi-\pi$ interactions) or with cationic residues in drugs (cation$-\pi$ interactions) (*22*). Recently, Sauna et al. (*25*) also suggested a variable number of binding interactions between substrate and transporter, however, without specifying the type of interactions. Concepts with a variable number of binding modules contrast with classical quantitative structure−activity relationship, QSAR, approaches (for review see refs *26*, *27*) or multivariant procedures (e.g. ref *28*) that are both based on "key-lock" concepts and consider one single "key" or "pharmacophore" per Pgp substrate.

Drug partitioning into the lipid membrane and drug binding to Pgp within the lipid membrane are tightly coupled processes which have not yet been deconvoluted satisfactorily. In the following we demonstrate that the binding constant of a given substrate in the lipid phase to the activating (inhibitory) binding region of Pgp, $K_{tl(1)}$ ($K_{tl(2)}$), can be calculated provided the corresponding lipid−water partition coefficient, K_{lw}, and the binding constant of the drug from the aqueous phase to the activating (inhibitory) binding region of Pgp, $K_{tw(1)}$ ($K_{tw(2)}$), are known. The binding constants from water to the transporter, $K_{tw(1)}$ ($K_{tw(2)}$), were determined in living NIH-MDR-G185 cells as the inverse of the concentrations of half-maximum Pgp activation, K_1 (inhibition, K_2) (*11*). The concentrations of half-maximum Pgp activation, K_1 (inhibition, K_2) were measured by means of a Cytosensor microphysiometer (*29*) that monitors the extracellular acidification rate, ECAR (*17*, *18*). As a control, we also measured the phosphate release rates upon drug-induced Pgp-ATPase activation in inside-out membrane vesicles and showed that the ECARs and the phosphate release rates are identical ((*18*), Äänismaa and Seelig, in preparation). The lipid−water partition coefficients, K_{lw}, were derived from the air−water partition coefficients, K_{aw}, and the cross-sectional area, A_D, of the drug taking into account the lateral packing density, π_M (*30*, *31*), and the surface potential, ψ, of the cytosolic membrane leaflet. The lipid−water partition coefficients, K_{lw}, obtained by means of this approach were in excellent agreement with the lipid−water partition coefficients obtained by means of isothermal titration calorimetry using model membranes of known lateral packing density (for the present compounds, Li-Blatter and Seelig, in preparation).

We selected 15 chemically diverse drugs (antidepressants, an antineoplastic, antipsychotics, a calcium channel blocker, local anesthetics, an immunosuppressant, a steroid hormone, a tyrosine kinase inhibitor) and report for the first time the binding constants of the drugs from the lipid membrane to the activating (inhibitory) binding region of the transporter in the lipid phase, $K_{tl(1)}$ ($K_{tl(2)}$). The corresponding free energies of binding, $\Delta G°_{tl(1)}$ ($\Delta G°_{tl(2)}$), reflect the *effective* interactions between the substrates and the activating (inhibitory) binding region of Pgp. We show that the substrate concentrations in the membrane are higher by a factor of 10^2 to 10^4 than those in the aqueous phase, which implies that the interactions between drugs and Pgp in the lipid membrane are relatively weak. Our results further indicate that binding of drugs to Pgp is not compatible with a classical "key-lock" or "one-pharmacophore" model but can be well explained with a modular binding concept, where the energetically most relevant binding module seems to consist of two hydrogen bond acceptor groups.

MATERIALS AND METHODS

Materials. Amitriptyline·HCl, *cis*-flupenthixol·2HCl, daunorubicin·HCl, dibucaine·HCl, diltiazem·HCl, lidocaine·HCl, progesterone, promazine·HCl, trifluoperazine·2HCl, and triflupromazine·HCl were from Sigma-Aldrich (Steinheim, Germany), and (*R*/*S*)-verapamil·HCl was from Fluka (Buchs, Switzerland). Chlorpromazine·HCl and reserpine·HCl·H_2O were generous gifts from Merck (Darmstadt, Germany), and cyclosporin A and glivec mesylate from Novartis AG (Basel, Switzerland). For Cytosensor measurements cyclosporin A, progesterone, reserpine, and (*R*/*S*)-verapamil were dissolved in DMSO, where the final DMSO concentration did not exceed 0.5% (v/v). The remaining drugs were directly dissolved in medium. To test the influence of DMSO on membrane partitioning and Pgp binding, (*R*/*S*)-verapamil and glivec were measured with and without DMSO. The results were identical within error limits (Äänismaa and Seelig, in preparation). Cell culture medium DMEM with pyruvate (liquid and dry, Cat. No. 21969 and Cat. No. 52100, respectively) as well as other compounds required for cell culture such as fetal bovine serum, FBS, L-glutamine, and antibiotics were from Gibco-BRL (Basel, Switzerland).

Buffers. Buffers were adjusted to pH 7.4 at ambient temperature. For Cytosensor measurements (performed at 37 °C), a flow medium with low buffer capacity is required. The flow medium was prepared from dry powder Dulbecco's modified Eagle medium (Gibco-BRL, Basel, Switzerland) which contains 0.91 mM phosphate but no sodium bicarbonate. Flow medium was supplemented with 1 mM sodium pyruvate to decrease the basal ECAR of cells and to enhance the relative ECAR changes due to Pgp activation in particular (*18*). In order to preserve osmotic balance the lacking sodium bicarbonate was replaced by sodium chloride (2.6 g/L of NaCl instead of 3.7 g/L of $NaHCO_3$).

Cell Lines and Cell Culture. The mouse embryo fibroblast cell lines NIH3T3 and NIH3T3 transfected with the human *MDR1* gene, NIH-MDR-G185 (grown in the presence of 0.15 μM colchicine), were generous gifts from Dr. M. M. Gottesman and Dr. S. V. Ambudkar (The National Institutes of Health, Bethesda, MD). Cells were maintained as described earlier (*17*, *18*).

Cytosensor Measurements. In short, the Cytosensor microphysiometer measures the rate of proton excretion from 10^4 to 10^6 cells in a flow chamber with diffusive contact to a pH sensitive silicon chip. Due to the flow chambers it is possible to maintain approximately constant drug concentrations, which allows the establishment of steady state conditions. Cytosensor measurements with NIH3T3 and NIH-MDR-G185 cells and the quantification of extracellular acidification are described elsewhere in detail (*17*, *18*). In the present study the drug concentrations were corrected for adsorption to the walls of the fluid supply tubes, the debubbler membranes, and the flexible tubing (∼65 cm) which connect the fluid supply tubes with the Cytosensor

chamber. Corrections were made in separate control runs by sampling the drug solution just before entering the sensor chamber and measuring the drug concentration by UV spectroscopy. To mimic the time schedule of Cytosensor measurements the drug solutions were let to flow through Cytosensor tubing 6 min before the samples were collected during the 3 min. Adsorption varied strongly from compound to compound and was small for verapamil and high for phenothiazines. Cyclosporin A concentrations could not be corrected for adsorption by UV because the molecule does not contain UV-detectable amino acid residues.

Lipid−Water and Air−Water Partition Coefficient. Measurement of the lipid−water partition coefficient, K_{lw}, in intact cells is not possible since other structures e.g. the glycocalix or proteins also attract cationic compounds. We have therefore developed an approach that allows determination of the lipid−water partition coefficient, K_{lw}, from the air−water partition coefficient, K_{aw}, and the cross-sectional area, A_D, of the drug, by taking into account the relevant lateral membrane packing density, π_M (*30*, *31*), and the surface potential of the membrane, ψ. The air−water partition coefficient, K_{aw}, and the cross-sectional area, A_D, of the drug were derived from measurements of the surface pressure, π, as a function of concentration (Gibbs adsorption isotherm) as described previously ((*30*, *31*), for the present compounds, Li-Blatter and Seelig, in preparation).

The Kinetic Models. The kinetics of Pgp activation has been discussed in detail elsewhere (*11*, *17*) and is summarized briefly. The model used to analyze Pgp−drug interactions is outlined in the scheme depicted in eq 1. In

$$\begin{array}{ccccccc} & K_{lw} & & K_{tl(1)} & & K_{tl(2)} & \\ & k_0 & & k_1 & S_l\ k_2 & & \\ S_w & \rightleftharpoons & S_l + T(ATP) & \rightleftharpoons & T(ATP)S_t & \rightleftharpoons & T(ATP)S_tS_t \\ & k_{-0} & & k_{-1} & & k_{-2} & \end{array} \qquad (1)$$

$$\downarrow k_{bas} \qquad \downarrow k_{cat}' \qquad \downarrow k_{cat}''$$

$$T(ADP) + P_i + H^+ + S_{rel}$$

$$T(ADP)S_t + P_i + H^+ + S_{rel} \quad \text{or}$$

$$T(ADP) + P_i + H^+ + 2S_{rel}$$

the *absence* of exogenous substrates Pgp shows basal activity, with k_{bas} as the catalytic rate constant (1st arrow down). Substrates in the aqueous phase, S_w, partition into the lipid membrane, where k_0 and k_{-0} are the partitioning rate constants, and $K_{lw} = k_0/k_{-0}$ is the lipid−water partition coefficient. The substrate in the lipid membrane, S_l, binds to the transporter, T, forming the transporter−ATP−substrate complex, $T(ATP)S_t$ (for simplicity only one ATP (ADP) molecule per Pgp is shown in eq 1); S_t is the substrate bound to the activating binding region of the transporter, k_1 and k_{-1} are the rate constants for association to and dissociation from the activating binding region, and $K_{tl(1)} = k_1/k_{-1}$ is the binding constant of the substrate for the activating binding region of the transporter within the lipid membrane. The 2nd arrow down shows the substrate transport step which is driven by hydrolysis of ATP to ADP and phosphate, P_i, where k_{cat}' denotes the catalytic rate constant and S_{rel} the substrate released. At high substrate concentrations a second substrate molecule is bound to the inhibitory binding region forming the complex $T(ATP)S_tS_t$, where k_2 and k_{-2} are the association and dissociation rate constants, respectively, $K_{tl(2)} = k_2/k_{-2}$ reflects the binding constant to the inhibitory binding region of the transporter, and k_{cat}'' is the catalytic rate constant of the inhibitory binding step. The association/dissociation reactions are rapid compared to the catalytic steps (cf. ref *32*) (k_{-1} and $k_{-2} \gg k_{bas}$, k_{cat}', k_{cat}''). To a first approximation, the concentration of half-maximum (minimum) activation K_1 (K_2) can therefore be assumed to correspond to the dissociation constant of the activating (inhibitory) binding region of Pgp and the inverse, $1/K_1$ ($1/K_2$), to the transporter−water binding constant for the activating (inhibitory) binding region, $K_{tw(1)}$ ($K_{tw(2)}$).

Based on this mechanism the following rate equation for ATP hydrolysis has been developed by Litman et al. (*14*):

$$V_{sw} = \frac{K_1K_2V_{bas} + K_2V_1C_{sw} + V_2C_{sw}^2}{K_1K_2 + K_2C_{sw} + C_{sw}^2} \qquad (2)$$

where V_{sw} is the rate of P_i release as a function of the substrate concentration in aqueous solution, C_{sw}, V_{bas} is the basal activity of Pgp in the absence of drug, V_1 is the maximum transporter activity (if only activation occurred), and V_2 is the minimum activity at infinite substrate concentration. At a substrate concentration, $C_{sw} = K_1$, half-maximum binding of the activating binding region is reached, and at a substrate concentration, $C_{sw} = K_2$, half-maximum binding of the inhibitory binding region is reached. Equation 2 is thus based on the concept of substrate inhibition (or uncompetitive inhibition) which was extended to allow for basal activation in the absence of a substrate and for breakdown of the complex $T(ATP)S_tS_t$ (eq 1). The kinetic data given in Table 1 were analyzed using this model.

For comparison we discuss a simplified version of the above model (*14*) that does not allow for catalytic activity of the complex $T(ATP)S_tS_t$ ($V_2 = 0$) and shows the following rate equation:

$$V_{sw} = \frac{K_1K_2V_{bas} + K_2V_1C_{sw}}{K_1K_2 + K_2C_{sw} + C_{sw}^2} \qquad (3)$$

A related model was proposed by Al-Shawi et al. (*33*, *34*). It also considers basal activation of Pgp in the absence of drugs, drug activation, and drug inhibition. However, it is based on the concept of noncompetitive inhibition and shows the following rate equation:

$$V_{sw} = \frac{K_1K_2V_{bas} + K_2V_1C_{sw}}{K_1K_2 + K_1C_{sw} + K_2C_{sw} + C_{sw}^2} \qquad (4)$$

The influence of the different models on the kinetic data will be discussed.

The Thermodynamics of Substrate Binding. As shown previously (*11*), the binding constant of the drug from water to the transporter, $K_{tw(1)}$, is the product of the lipid−water partition coefficient, K_{lw}, and the binding constant of the drug from the lipid membrane to the transporter, $K_{tl(1)}$,

$$1/K_1 \cong K_{tw(1)} \cong K_{tl(1)}K_{lw} \qquad (5)$$

This leads to the corresponding free energy relationship

$$\Delta G^\circ_{tw(1)} \cong \Delta G^\circ_{tl(1)} + \Delta G^\circ_{lw} \qquad (6)$$

where the degree symbol refers to a biological standard state

Table 1: Thermodynamic and Kinetic Parameters for 15 Drugs[a]

no.	compound	pK_a	K_{aw} [mM^{-1}] pH 7.4	A_D [Å^2] pH 8.0	K_1 [μM]	K_2 [μM]	V_1 [fold]	V_2 [fold]	$X_{b(1)}$ [mmol/mol]	$X_{b(2)}$ [mmol/mol]	weighted number H-bond acceptors	ΔG°_{Hi} [kJ/mol]
1	amitriptyline	9.4(53)	7.1(30)	52(15)	6.4 ± 0.2	57.2 ± 11.3	1.9 ± 0.01	0.2 ± 0.2	3.6	33.5	2	−7.0
2	chlorpromazine	9.2(54)	21.5(30)	42(30) (pH 7.4)	5.7 ± 0.0	16.4 ± 3.0	2.0 ± 0.3	0.0 ± 0.0	20.2	58.1	2	−4.9
3	*cis*-flupenthixol	7.8(55)	453(30)	60(30)	3.0 ± 1.8	33.8 ± 18.1	1.4 ± 0.2	0.0 ± 0.0	47.0	523.0	2.5	−3.1
4	cyclosporin A	-	19952.6(15)	140	0.02 ± 0.01	1.5 ± 1.0	1.1 ± 0.1	0.8 ± 0.3	0.02	1.6	10.5	−2.6
5	daunorubicin	8.4(56)	588.8(15)	106(15)	0.6 ± 0.3	19.0 ± 4.0	1.1 ± 0.05	0.1 ± 0.1	0.6	19.1	7	−2.6
6	dibucaine	8.5(57)	11.3	52	10.9 ± 1.0	21.0 ± 7.8	2.0 ± 0.2	1.0 ± 0.1	9.4	18.2	1.5	−7.8
7	diltiazem	8.9(58)	26.9(15)	70(15)	3.5 ± 0.4	296.8 ± 107.6	1.8 ± 0.2	0.8 ± 0.2	2.2	182.0	3.5	−4.4
8	glivec	8.07	198	98	2.9 ± 2.7	117.8 ± 25.3	1.2 ± 0.1	0.0 ± 0.0	1.6	63.1	3	−5.4
9	lidocaine	7.6(59)	2.9(30)	50	375.6 ± 91.3	nd	1.5 ± 0.1	nd	66.7	nd	1.5	−4.5
10	progesterone	-	157	40[b]	5.0 ± 0.7	12.4 ± 1.9	1.7 ± 0.2	1.2 ± 0.2	47.4	117.9	1.5	−5.1
11	promazine	9.42(60)	4.8	42(31)	78.7± 22.0	131.5 ± 11.0	3.7 ± 0.6	0.0 ± 0.0	62.9	105.0	2	−3.5
12	(*R*/*S*)-verapamil	8.92(61)	166.0(15)	90	0.5 ± 0.1	37.3 ± 15.3	1.6 ± 0.1	1.1 ± 0.1	0.4	34.8	5	−3.9
13	reserpine	6.6(62)	2030	99	0.3 ± 0.1	10.7 ± 1.5	1.3 ± 0.1	0.6 ± 0.2	0.6	24.9	8	−2.3
14	trifluoperazine	8.09(63)	342	57.4(31)	3.6 ± 0.0	21.8 ± 3.2	1.6 ± 0.1	0.0 ± 0.0	57.4	349.0	2.5	−2.9
15	triflupromazine	9.1(64)	91.1	50(31)	2.0 ± 0.5	31.1 ± 1.6	1.7 ± 0.1	0.0 ± 0.0	17.0	266.3	2.5	−4.1

[a] The air−water partition coefficient, K_{aw}, and the cross-sectional area, A_D, were obtained by means of surface activity measurements. The concentration of half-maximum activation (inhibition), K_1 (K_2), and of maximum (minimum) transporter activity, V_1 (V_2), were measured in living NIH-MDR-G185 cells with a Cytosensor. The mole fraction of drugs in the membrane at half-maximum Pgp activation (inhibition), $X_{b(1)}$ ($X_{b(2)}$), was calculated according to eq 20 using the lipid−water partition coefficients, K_{lw} (Figure 4A), calculated by means of eq 12 assuming a membrane packing density of $\pi_M = 30$ mN/m and a surface potential of the cytosolic leaflet of $\psi = -30$ mV. The number of H-bond acceptors and the free energy of binding per H-bond, ΔG°_{Hi}, was determined as described in Discussion. [b] The cross-sectional area of progesterone was estimated in analogy to the cross-sectional area of cholesterol. The error in the surface activity measurements is generally not larger than ±5%. However, for compounds with low amphiphilicity (e.g. daunorubicin, progesterone) the air−water partition coefficient as well as the cross-sectional area of the molecule can be affected by the association state of the molecule in solution which depends on the stock solution concentration and data variation can therefore be larger. Data presented in Table 1 correspond to average values of 1−4 data sets made with cells of different passages (cell passage number > 4), where one data set consists of 2−3 measurements made with cells of the same passage number as shown in Figure 3.

(pH 7.4 and 37 °C). The free energy of substrate binding from water to the transporter, $\Delta G^\circ_{tw(1)}$, and the free energy of partitioning into the lipid membrane, ΔG°_{lw}, are defined as

$$\Delta G^\circ_{tw(1)} \cong -RT \ln(C_w K_{tw(1)}) \cong -RT \ln(C_w(1/K_1)) = RT \ln(C_w K_1) \quad (7)$$

and

$$\Delta G^\circ_{lw} = -RT \ln(C_w K_{lw}) \quad (8)$$

respectively, where C_w corresponds to the molar concentration of water. Analogous equations can be formulated for the binding constant and the free energy of binding to the second binding region,

$$1/K_2 \cong K_{tw(2)} \cong K_{tl(2)} K_{lw} \quad (9)$$

and

$$\Delta G^\circ_{tw(2)} \cong \Delta G^\circ_{tl(2)} + \Delta G^\circ_{lw} \quad (10)$$

where K_2 is the dissociation constant, $K_{tw(2)}$ and $K_{tl(2)}$ are the binding constant from water and from the lipid membrane to the inhibitory binding region of Pgp, respectively, and $\Delta G^\circ_{tw(2)}$ and $\Delta G^\circ_{tl(2)}$ are the corresponding free energies.

RESULTS

Drug-Induced Pgp Activation Measured in MDR1-Transfected and Wild-Type Cells. MDR1-transfected (NIH-MDR-G185) and wild type (NIH3T3) mouse embryo fibroblasts were exposed to 15 chemically diverse drugs (cf. Table 1), and the extracellular acidification rate, ECAR, was measured by means of the Cytosensor. Figure 1 shows a comparison of the raw data (A and B, where A is an enlargement of B) and the rate data (C) obtained upon exposure of NIH-MDR-G185 and wild-type cells to chlorpromazine (3.4 μM). During each 120 s pump cycle, buffer was superfused for 100 s, then the pumps were switched off for the remaining 20 s, and the pH change was measured during 13 s within this time. When the pumps were on, the acidic metabolites excreted by the cells were washed away by the flow of medium, and the pH at the cell surface therefore remained constant and was identical to the pH of the flow medium. During pump-off periods (20 s) acidic products accumulated in the sensor chambers, causing a decrease of the pH. The ECAR was determined during 13 s of the pump-off period as the slope of a linear least-squares fit to voltage versus time data ($-\mu$V/s) (rate data), where -1 μV/s corresponds to an acidification rate of 1 mpH unit/min at pH 7.4 (Figure 1A). During the first four pump cycles cells were exposed to the flow medium without chlorpromazine and the basal ECAR was measured as seen in Figure 1B and 1C. Next NIH-MDR-G185 and NIH3T3 cells were exposed to a chlorpromazine-containing (3.4 μM) medium for a 40 s pulse and the ECAR was measured. Perfusion with chlorpromazine solution was continued for another 100 s and the ECAR was measured again. The hatched region in Figures 1B and 1C indicates the drug-stimulation period of 180 s comprising two measuring points. In the following, the second measuring point (filled symbol) was used for data evaluation for all compounds except cyclosporin A which was stimulated for a longer period of time (11 min). Drug stimulation for longer periods of time generally did not change the ECAR indicating that steady state conditions were reached.

After stimulation with drug-containing medium the cells were again perfused with flow medium and the ECAR measurements were continued every two minutes until basal

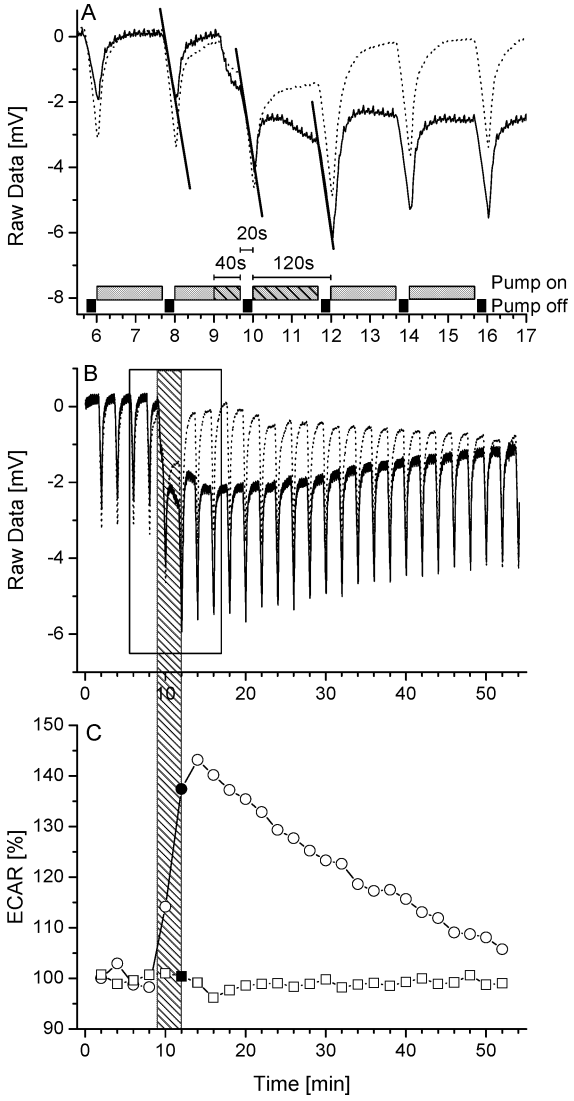

FIGURE 1: (A−C) ECAR measured by means of a Cytosensor microphysiometer. *MDR1*-transfected (NIH-MDR-G185) (solid lines in Figures 1A and B, circles in Figure 1C) and wild-type cells (NIH3T3) (dotted lines in Figures 1A and B, squares in Figure 1C) were exposed to 3.4 μM chlorpromazine. (A) Raw data show changes of the voltage (mV) with time, that are proportional to pH changes (-1 μV/s = 0.001 pH unit/min at pH 7.4). When the pumps are on (gray boxes), the pH in the measuring chamber corresponds to the pH of flow medium. When the pumps are off (black boxes), the pH drops due to an accumulation of acidic metabolites in the extracellular environment. Gray hatched boxes indicate the stimulation period of cells with chlorpromazine and comprise two measurements, where the second measurement (180 s) indicated by a filled symbol (C) is used for data evaluation. (B) Same data as in part A shown on a longer time scale. (C) Rate data show the acidification rate ($-\mu$V/s) in time, determined by a least-squares fit to the slope from the raw data when pumps are off. Values are normalized to the basal ECAR defined as 100%.

rates were reached again. The acidification rate was normalized to the basal acidification rate (average of the first four pump cycles before drug addition) which was defined as 100%. It has to be noted that the basal ECAR is the sum of the Pgp basal activity and other metabolic processes. The cellular response is given as the percentage of the basal activity (Figure 1C). As seen in Figures 1B and 1C addition of chlorpromazine to the flow medium leads to an ECAR increase in NIH-MDR-G185 cells, but not in wild-type cells.

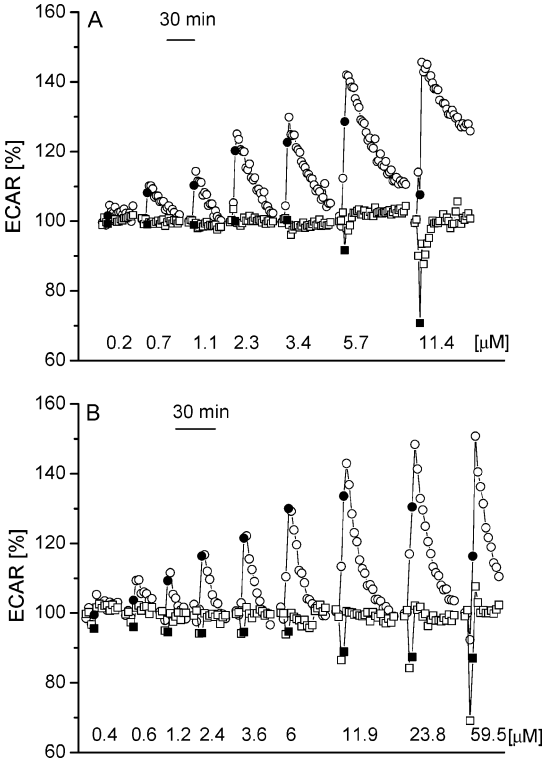

FIGURE 2: (A, B) Time-dependent ECAR of NIH-MDR-G185 (circles) and NIH3T3 (squares) cells in response to increasing concentrations of chlorpromazine (A) and dibucaine (B). The cells were stimulated with drugs for 180 s. Each segment is normalized to a basal acidification rate (the average of the two data points of the ECAR before drug addition defined as 100%). The second stimulation point obtained during the drug-stimulation period is indicated by a filled symbol and is used for data evaluation. The subsequent open circles correspond to measurements performed in the presence of drug-free medium. Measurements were continued until the ECAR returned to basal values. At low drug concentrations, where only the activating binding region of Pgp is occupied, the second stimulation point (filled symbol) corresponds to the ECAR maximum. At high drug concentrations the ECAR at the second stimulation point (180 s) is lower than the ECAR at the subsequent (third) stimulation point. This is due to the fact that reperfusion of the cells with drug-free medium lowers the membrane concentration of drugs which leads to the release of the substrate molecule at the inhibitory binding region of Pgp.

Figure 2 displays the ECAR changes relative to the basal acidification rates of NIH-MDR-G185 (circles) and NIH3T3 cells (squares) upon stimulation with either chlorpromazine (A) or dibucaine (B) at different concentrations as a function of time. The second measuring point at the end of the drug-stimulation period (at 180 s) is again indicated by a filled symbol (Figures 1C, 2A, and 2B).

The response of wild type cells (Figures 2A and 2B) was negligibly small for all drugs at low concentrations ($C < 10$ μM). Some drugs induced a fast transient decrease of the ECAR (to maximally ~70%) at high concentrations as seen in Figures 2A and 2B. The largest transient effects were observed for chlorpromazine and dibucaine, which are given as examples in Figures 2A and 2B. Due to the protection of the cells by Pgp this effect was small in NIH-MDR-G185 cells. At high concentrations, $C > 10$ μM, the cytotoxic daunorubicin induced metabolic changes in wild-type cells which were similar to those in *MDR1*-transfected cells.

Analysis of Pgp Activation. Plotting the ECARs of NIH-MDR-G185 cells at the end of the drug-stimulation period

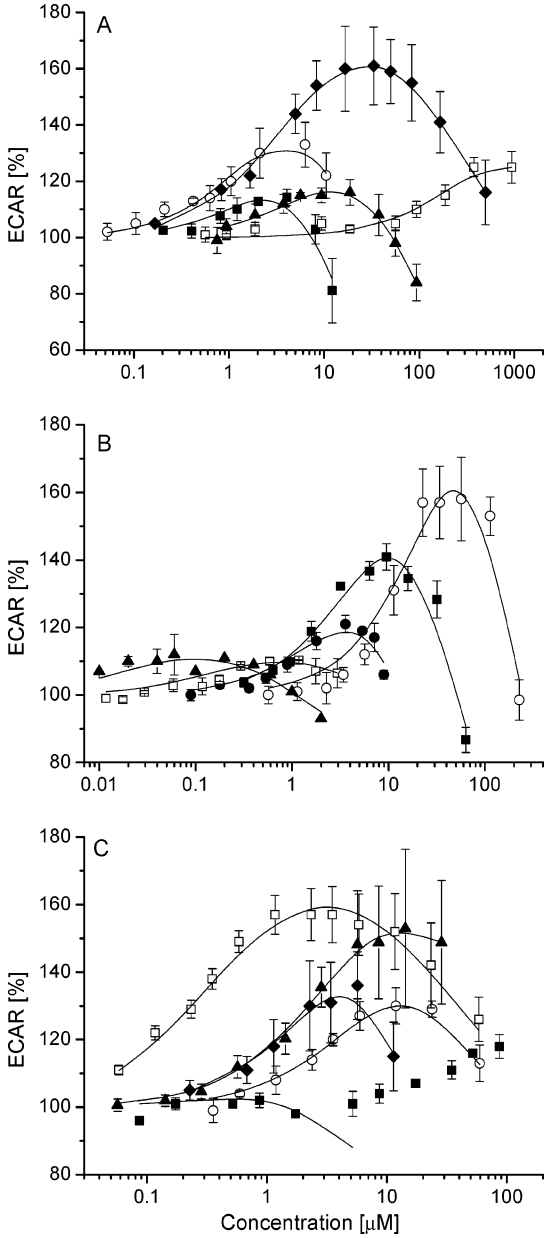

FIGURE 3: (A−C) Pgp activation profiles obtained by ECAR measurements in NIH-MDR-G185 cells stimulated by *cis*-flupentixol (■), diltiazem (◆), glivec (▲), lidocaine (□), triflupromazine (○) (A), amitriptyline (■), cyclosporin A (▲), promazine (○), reserpine (□), and trifluoperazine (●) (B), chlorpromazine (◆), daunorubicin (■) (data in the low concentration range $C < 5\ \mu$M are fitted to eq 2, metabolic changes due to effects other than Pgp activation are observed at $C > 10\ \mu$M), dibucaine (○), progesterone (▲), and verapamil (□) (C). The solid lines are fits to eq 2 assuming activation with one and inhibition with two drug molecules bound to Pgp. Symbols represent average value of $n = 2-3$ measurements with cells of the same cell passage.

at 180 s (indicated by solid symbols in Figures 1C, 2A, and 2B) as a function of the logarithm of concentration yields activation profiles as displayed in Figure 3. The Pgp activation profiles of all drugs show a characteristic bell-shaped dependence on the logarithm of concentration, in agreement with previous investigations in other cell lines (*14*, *17*), as well as in reconstituted proteoliposomes (*33*). The solid lines are fits to the modified Michaelis−Menten equation (eq 2) assuming Pgp activation upon binding of a first drug molecule at low, and inhibition upon binding of a second drug molecule at high, concentration. The error bars in Figures 3A−C correspond to the average of two to three measurements made with cells of the same passage (one data set). For compounds which are especially prone to aggregation, such as phenothiazines (e.g. chlorpromazine (*31*)) and progesterone, the quality of data decreases with increasing concentration as reflected in an increase in error bars. Data were evaluated using an automated fit program to eq 2 (described elsewhere, Äänismaa and Seelig, in preparation) yielding the concentration of half-maximum activation, K_1, and inhibition, K_2, as well as the maximum, V_1, and minimum rate, V_2, of Pgp activity. Data obtained with NIH-MDR-G185 are summarized in Table 1 and correspond to average values of one to four data sets made with cells of different passages. For the present study the cell passage number was $n > 4$ (*18*).

Binding to the Inhibitory Region of Pgp Is Reversible. A closer inspection of Figures 2A and 2B is now possible. It reveals that the data point at the end of the drug-stimulation period (at 180 s) is identical with the ECAR maximum at low drug concentrations. At higher drug concentrations the ECAR maximum is observed at the subsequent measuring point. At this point the cells have been reperfused with drug-free medium for 100 s (plus 20 s measuring stop) and the concentration of the drug in the membrane has therefore decreased below the value at which the inhibitory binding region is occupied. The increase in the ECAR is thus due to the release of the inhibitory substrate molecule from Pgp, which directly prooves the reversibility of the inhibitory binding step in eq 1.

Figure 2A further shows that more than 1 h can be required to reach the basal ECAR after reperfusion with drug-free medium. This implies that the membrane concentration of drugs in *MDR1*-transfected cells decreases only slowly (as discussed in detail elsewhere).

Drug Partitioning into the Lipid Membrane. For the electrically neutral extracellular lipid leaflet the lipid−water partition coefficient, K_{lw}, can be derived from the air−water partition coefficient, K_{aw}, and the cross-sectional area of the drug molecule in its amphiphilic orientation at the air−water interface, A_D ((*30*, *31*), for the present compounds, Li-Blatter and Seelig, in preparation),

$$K_{lw} = K_{aw}\, e^{-\pi_M A_D/kT} \qquad (11)$$

where $\pi_M A_D$ is the energy required to create a cavity with a cross-sectional area, A_D, in a membrane exhibiting the lateral packing density, π_M, and kT is the thermal energy per molecule (*35*). The air−water partition coefficient, K_{aw}, was determined at pH 7.4. The cross-sectional area, A_D, was measured at pH 8.0 to minimize charge repulsion effects (*30*, *31*). The lateral packing density, π_M, of mouse embryo fibroblasts was determined as $\pi_M \approx 30$ mN/m (cf. next paragraph).

After insertion into the outer, electrically neutral membrane leaflet, the neutral fraction of drugs rapidly crosses the hydrophobic core region and accumulates in the inner, cytosolic membrane leaflet. The polar groups of the drug then reside in the headgroup region of the lipids, and the hydrophobic groups remain in the hydrophobic core. The cytosolic lipid leaflet contains ∼25% negatively charged lipids and thus exhibits a negative surface potential, ψ. Since

it is generally assumed that Pgp binds its substrates when they are inserted in the cytosolic membrane leaflet (although other binding locations have been proposed (*36*)), we calculated the appropriate cytosolic lipid−water partition coefficient by taking into account the charge, *z*, of the drug and the surface potential, ψ, of the cytosolic membrane leaflet,

$$K_{lw} = K_{aw}\, e^{-\pi_M A_D/kT}\, e^{-\psi Fz/RT} \qquad (12)$$

where *RT* is the thermal energy per mole, and *F* the Faraday constant.

The surface potential, ψ, depends not only on the lipid composition of the membrane but also on the cytosolic ion concentration. The cytosolic free magnesium concentration has been estimated to be in the range of $C = (0.5 \text{ to } 1)$ mM (*37*), and the concentration of monovalent cations is in the range of $C = (100 \text{ to } 150)$ mM. With a binding constant of $K = 10\ M^{-1}$ and $K = 0.6\ M^{-1}$ for magnesium and for monovalent cations, respectively (*38*), a surface potential in the range of $\psi \approx (-30 \text{ to } -20)$ mV is calculated using the Gouy−Chapman theory (*39*). Binding of cationic drugs also reduces the membrane surface potential. For most drugs it reaches a value of $\psi \approx 0$ mV at the concentration of half-maximum Pgp activation. To illustrate the effect of the surface potential we calculated the lipid water partition coefficients, K_{lw}, for the two extreme values, $\psi = 0$ mV, and $\psi = -30$ mV.[2] As seen in Figure 4A the lipid−water partition coefficients were in the range of $K_{lw} = (10^2 \text{ to } 10^4)\ M^{-1}$ and $K_{lw} = (2 \times 10^2 \text{ to } 2 \times 10^4)\ M^{-1}$ for $\psi = 0$ mV, and $\psi = -30$ mV, respectively. The lipid−water partition coefficients, K_{lw}, of the different drugs thus vary by 2 orders of magnitude under both conditions, whereas an increase of the negative surface potential from $\psi = 0$ mV to $\psi = -30$ mV increases the lipid−water partition coefficient only by maximally a factor of about two. If not otherwise stated the following data are calculated with a negative surface potential, $\psi = -30$ mV.

The Lateral Packing Density, π_M, of the Plasma Membrane of NIH-MDR-G185 Cells. The lateral packing density, π_M, of a membrane cannot be measured directly; however, it can be determined in relation to a monolayer or bilayer with a known lateral packing density (*40*). As seen from eq 11 the lipid−water partition coefficient, K_{lw}, decreases exponentially with increasing lateral packing density, π_M, of the membrane (*35*, *41*). If the lipid−water partition coefficients, $K_{lw(A)}$ and $K_{lw(B)}$, and the surface potential difference, $\psi_B - \psi_A$, of two membranes, A and B, are known, the packing density difference between the two membranes, $\pi_{M(B)} - \pi_{M(A)}$, can be determined as

$$(\pi_{M(B)} - \pi_{M(A)}) = \frac{kT}{A_D}\left(\ln\left(\frac{K_{lw(A)}}{K_{lw(B)}}\right) - \frac{Fz}{RT}(\Psi_B - \Psi_A)\right) \qquad (13)$$

In the comparison of cells the surface potential difference can be neglected to a first approximation and the last term in eq 13 thus cancels. With a reference membrane, A, of known packing density, $\pi_{M(A)}$, the packing density of the cell membrane, B, $\pi_{M(B)}$, can then be evaluated.

According to eq 5 the binding constant of the substrate from water to the transporter, $K_{tw(1)}$ (or $1/K_1$), corresponds to the product of the lipid−water partition coefficient and the binding constant of the substrate from the lipid membrane to the transporter, where $K_{tl(1)}$ is likely to be packing density independent (cf. Discussion). The binding constant of the substrate from water to the transporter, $K_{tw(1)}$, thus shows the same exponential dependence on the membrane packing density, π_M, as the lipid−water partition coefficient, K_{lw}. Therefore, the packing density difference, $\pi_{M(B)} - \pi_{M(A)}$, between two different cell membranes, A and B, can be evaluated by measuring the concentrations of half-maximum activation, $K_{1(A)}$ and $K_{1(B)}$, of Pgp embedded in two different membranes,

$$(\pi_{M(B)} - \pi_{M(A)}) = \frac{kT}{A_D}\left(\ln\left(\frac{K_{1(B)}}{K_{1(A)}}\right) - \frac{Fz}{RT}(\Psi_B - \Psi_A)\right) \qquad (14)$$

where the surface potential difference can again be neglected

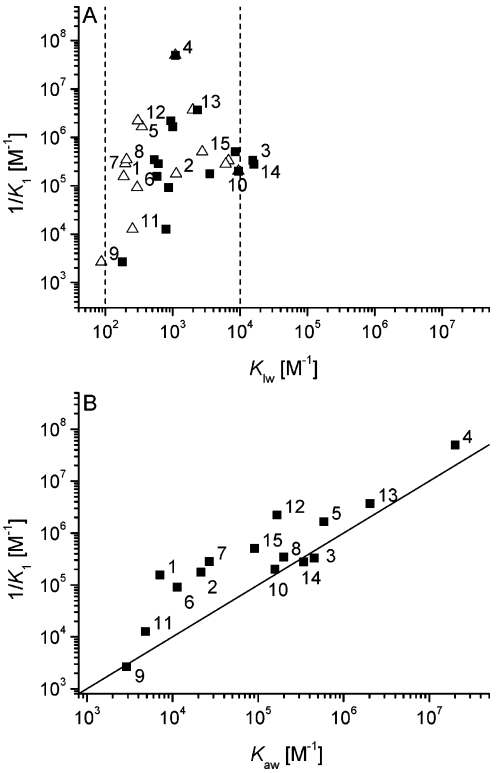

FIGURE 4: The inverse of the concentration of half-maximum Pgp activation, $(1/K_1)$, obtained by measurements of the ECAR in NIH-MDR-G185 cells, is plotted as a function of the lipid−water partition coefficient, K_{lw} (A), and as a function of the air−water partition coefficient, K_{aw} (B). Open triangles and filled squares in Figure 4A refer to a membrane surface potential, $\psi = 0$ mV and $\psi = -30$ mV, respectively. Surface activity measurements were performed at pH 7.4. (1) amitriptyline, (2) chlorpromazine, (3) *cis*-flupenthixol, (4) cyclosporin A, (5) daunorubicin, (6) dibucaine, (7) diltiazem, (8) glivec, (9) lidocaine, (10) progesterone, (11) promazine, (12) (R/S)-verapamil, (13) reserpine, (14) trifluoperazine, and (15) triflupromazine. The straight line in Figure 4B exhibits a slope $m = 1$.

[2] Inside-out plasma membrane vesicles of *MDR1*-transfected (NIH-MDR-G185) and wild-type cells (NIH3T3) exhibit the same ζ-potential. The ζ-potential of the inside-out plasma membrane vesicles is moreover similar to that of the intact cells from which they were derived. The negative ζ-potential of inverted plasma membrane vesicles is due to the negatively charged lipids in the cytosolic membrane leaflet, and that of intact cells is due essentially to the extracellular glycocalix located above the level of electrically neutral lipid headgroups. In the absence of drugs the ζ-potential is (-23 ± 3) mV (E. Gatlik, X. Li-Blatter, A. Seelig, unpublished results) and is thus in good accordance with the surface potential, ψ, used in the present investigation.

Table 2: The Lateral Membrane Packing Density, π_M, of Different Pgp Containing Membranes Estimated by Comparing Concentrations of Half-Maximum Pgp Activation K_1 (or K_m) by Verapamil[a]

membrane	rate equation	K_1 (or K_m) [μM]	Mg^{2+} [mM]	ATP [mM]	π_M [mN/m]	ψ [mV]	K_{lw} [M^{-1}]	$X_{b(1)}$ [mmol/mol]
lipid (DMPC)(13)	Michaelis−Menten equation	0.63[b]			30(42)	0	336	0.21
NIH-MDR-G185 cells	eq 2	0.5	cellular	cellular	30.5	−20	514	0.26
LLC-MDR1 cells(17)	eq 2	0.89[c]	cellular	cellular	33	−20	307	0.27
CR1R12 cells(14)	eq 2	2.5	2.5	3	35.5	−20	101	0.25
lipid mixture with *E. coli* lipids[d] (43)	Michaelis−Menten equation	4.7	5	5−7.5	42	−20	51.3	0.24
lipid mixture with *E. coli* lipids[d] (33,45)	eq 4	30 62.2	15 15	10 10	48 51	−5 −5	8.3 4.4	0.25 0.27

[a] The K_1 (or K_m) values were taken from literature, and the corresponding experimental conditions (magnesium ion and ATP concentration, respectively, pH, and temperature) are given. The membrane packing density, π_M, was calculated according to eq 14 using the surface potential, ψ, estimated taking into account 25% negatively charged lipids and the free ion concentration in the different assays. The lipid−water partition coefficient, K_{lw}, was determined according to eq 12 using the relevant surface potential and lateral packing density. The mole fraction of drugs in the membrane at half-maximum Pgp activation, $X_{b(1)}$, was calculated according to eq 20. All measurements discussed were performed at T = 37 °C and pH 7.4 except those of ref. (*13*) (T > 30 °C), ref. (*14*) (pH 7.0) and ref. (*43*) (pH 6.8). K_1 values measured at lower pH were divided by a factor of 2 to correct for pH (cf. ref (*45*), and Äänismaa and Seelig, in preparation) and the Michaelis−Menten constant, K_m, in ref. (*43*) was doubled to adjust to a K_1 value. [b] Dissociation constant determined by fluorescence quenching. The corresponding concentration of half-maximum activation (*13*) obtained by means of an ATPase assay is slightly higher. [c] Corrected for adsorption to the Cytosensor tubes. [d] Lipid mixture (*E. coli* bulk phospholipids, phosphatidylcholine, phosphatidylserine, cholesterol) (60:17.5:10:12.5 w/w).

in most cases (cf. Table 2). To estimate the lateral packing density of the plasma membrane of different *MDR1*-transfected cell lines we used as reference membrane a DMPC bilayer for which the lateral packing density has been determined previously as $\pi_M = (30 \pm 1)$ mN/m (*42*). DMPC bilayers have been used to reconstitute Pgp and to measure the concentration of half-maximum Pgp activation, K_1, by verapamil (*13*). With the two reference values for DMPC bilayers (π_M and K_1 for verapamil) the lateral packing density of the plasma membranes of NIH-MDR-G185 cells was estimated as $\pi_M = 30.5 \pm 1$ mN/m. For comparison we estimated the packing density of two other cell membranes (LLC-MDR1 (*17*) and CR1R12 cells (*14*)) and of mixed lipid bilayers (~60% *Escherichia coli* lipids, ~17.5% egg phosphatidylcholine, 10% bovine brain phosphatidylserine and ~12.5% cholesterol) (*34*, *43*) used for Pgp reconstitution (cf. Table 2). The membrane packing densities, π_M, estimated for the different membranes are summarized in Table 2. The type of assays, the kinetic models (rate equations), and the experimental conditions (e.g. pH, magnesium and ATP concentrations) differ in the different investigations.

The lateral packing densities of the mammalian plasma membranes investigated were found to be in the range of $\pi_M \cong$ (30 to 35) mN/m, which is in good agreement with previous investigations (*40*). The lowest packing density was found for mouse embryo fibroblasts (NIH-MDR-G185), which is consistent with the low cholesterol content generally found in embryonic cell membranes (*44*), and the highest packing density was observed in *Ehrlich* ascites tumor cells, CR1R12. The packing density of lipid membranes containing a high percentage of *E. coli* lipids (*33*, *43*, *45*) was determined as $\pi_M = 46.5 \pm 4.5$ mN/m, which is distinctly higher than that of the mammalian plasma membranes. The high packing density is mainly due to the high percentage of phosphatidylethanolamines in *E. coli* lipids. Phosphatidylethanolamines exhibit smaller cross-sectional areas and therefore higher packing densities than the corresponding phosphatidylcholines (*46*). The high packing density of *E. coli* lipids is also reflected in their high phase transition temperature (*47*, *48*).

Correlation between the Concentration of Half-Maximum Pgp Activation and the Lipid−Water Partition Coefficient. Figure 4A shows the inverse of the concentration of half-maximum Pgp activation, $1/K_1$ (log scale), versus the lipid−water partition coefficient, K_{lw} (log scale). No linear correlation is observed. Since $\log(1/K_1)$ is proportional to the free energy of binding from water to the activating binding region of Pgp, $\Delta G°_{tw(1)}$, and $\log K_{lw}$ is proportional to the free energy of drug partitioning from water to the membrane, $\Delta G°_{lw}$, it can be concluded that no correlation exists between the drug affinity from water to the transporter and the drug affinity to the lipid membrane for the present set of structurally diverse drugs. The same conclusion was drawn previously from octanol−water partition coefficients (*14*).

Correlation between the Concentration of Half-Maximum Pgp Activation and the Air−Water Partition Coefficient. If the $\log(1/K_1)$ (proportional to $\Delta G°_{tw(1)}$) is plotted versus the logarithm of the air−water partition coefficient, $\log K_{aw}$ (proportional to $\Delta G°_{aw}$) an approximately linear correlation is obtained as shown in Figure 4B. The air−water partition coefficients, K_{aw}, cover a broad range from $K_{aw} \sim 10^3$ M^{-1} (very hydrophilic compounds) to $K_{aw} \sim 10^7$ M^{-1} (very hydrophobic compounds). The straight line in Figure 4 corresponds to the product of the air−water partition coefficient and the concentration of half-maximum Pgp activation,

$$K_{aw}K_1 = 1 \tag{15}$$

The free energy of moving the drug from water to air, $\Delta G°_{aw} = -RT \ln(C_w K_{aw})$, is thus approximately identical to the free energy of substrate binding from water to the transporter, $\Delta G°_{tw}$,

$$\Delta G°_{aw} \approx \Delta G°_{tw} \tag{16}$$

Rewriting eq 11 in a logarithmic form and combining it with eq 8 yields

$$\Delta G°_{aw} = \Delta G°_{lw} - \pi_M N_A A_D \tag{17}$$

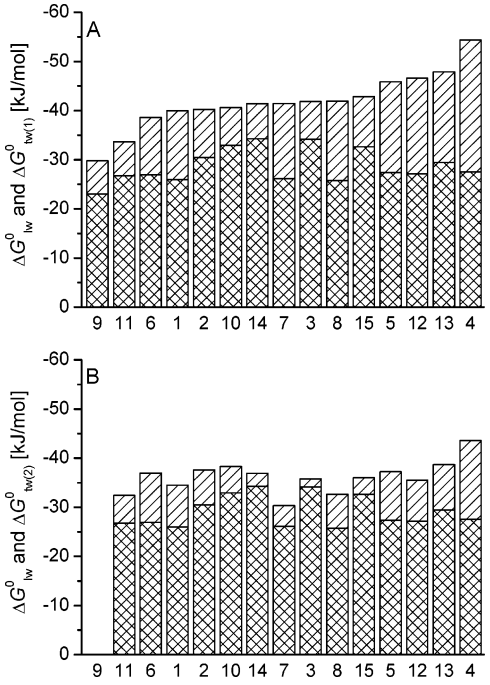

FIGURE 5: (A) The free energy of drug binding from water to the activating binding region of Pgp, $\Delta G°_{tw(1)}$ (hatched and crosshatched bars), in comparison to the free energy of drug partitioning from water to the lipid membrane, $\Delta G°_{lw}$ (crossed-hatched bars). The difference between $\Delta G°_{tw(1)}$ and $\Delta G°_{lw}$ represents the free energy of drug binding from lipid membrane to the transporter, $\Delta G°_{tl(1)}$ (hatched bar). (B) Analogous data for the inhibitory binding region of Pgp. Numbers correspond to those in Figure 4A. Lidocaine (9) is not included in Figure 5B since K_2 could not be precisely determined due to the high concentrations required (see Figure 3A).

where N_A is the Avogadro number. Equation 17 shows that the free energy of partitioning into the lipid−water interface, $\Delta G°_{lw}$, corresponds to the free energy of partitioning into the air−water interface, $\Delta G°_{aw}$, plus the additional work to penetrate into the lipid bilayers. Combining eqs 16 and 17 leads to the following approximation:

$$\Delta G°_{tw} \approx \Delta G°_{aw} = \Delta G°_{lw} - \pi_M N_A A_D \qquad (18)$$

or

$$\Delta G°_{tl(1)} \approx -\pi_M N_A A_D \qquad (19)$$

Equation 19 suggests that the free energy of binding to the transporter within the lipid membrane, $\Delta G°_{tl(1)}$, is proportional to the cross-sectional area of the molecule, A_D, as will be further discussed below (Figure 6A).

DISCUSSION

The thermodynamic and kinetic methods applied here were able to reveal the free energy of binding from water to the activating (inhibitory) binding region of Pgp in its native lipid membrane, $\Delta G°_{tw(1)}$ ($\Delta G°_{tw(2)}$), and the corresponding free energy of partitioning into the lipid membrane, $\Delta G°_{lw(1)}$, for 15 structurally diverse substrates. With this knowledge it is possible to determine two parameters which are not directly measurable, i.e., (i) the mole fraction of drugs in the membrane, $X_{b(1)}$ ($X_{b(2)}$), at half-maximum Pgp activation (inhibition) and (ii) the free energy of binding of the substrate from the lipid membrane to the activating, $\Delta G°_{tl(1)}$ (inhibitory, $\Delta G°_{tl(2)}$) binding region of Pgp. The latter reflects the direct

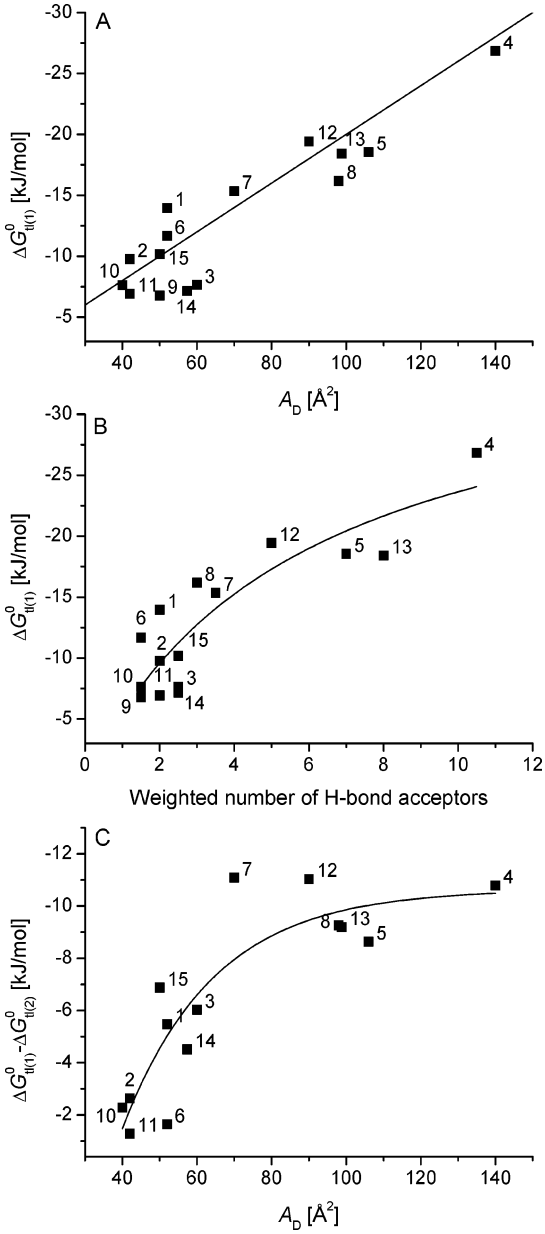

FIGURE 6: (A) The free energy of drug binding from the lipid membrane to the activating binding region of the transporter, $\Delta G°_{tl(1)}$, plotted as a function of the cross-sectional area, A_D, of the drug. A straight line corresponds to the diagonal. B: The free energy of drug binding from the lipid membrane to the activating binding region of the transporter, $\Delta G°_{tl(1)}$, as a function of the weighted number of hydrogen bond acceptors in patterns determined according to refs *10* and *23*. Data were fitted to a hyperbolic saturation isotherm. (C) The difference in the free energy of binding from water to the activating and inhibitory binding region of Pgp, $\Delta G°_{tl(1)} - \Delta G°_{tl(2)}$, plotted as a function of the cross-sectional area, A_D, of the drug. Data were fitted to an exponential curve. Numbers correspond to those in Figure 4. Values of $\Delta G°_{tl(1)}$ ($\Delta G°_{tl(2)}$) were obtained by means of ECAR measurements. Lidocaine (9) is not included in Figure 6C since K_2 could not be precisely determined due to the high concentrations required (see Figure 3A).

interplay between the drug and the transporter and provides the basis for a discussion of the nature of the interactions between Pgp and its substrates.

The Membrane Concentration of Drugs That Elicits Half-Maximum Pgp Activation. Biological membranes of different origin differ in their lipid composition and as a consequence in their lateral membrane packing density, π_M. As seen in

Table 2 the packing density of mammalian plasma membranes were found to be in the range of $\pi_M \cong$ (30 to 35) mN/m, whereas the packing density of membranes with a high percentage of *E. coli* lipids was distinctly higher, $\pi_M = 46.5 \pm 4.5$ mN/m. The membrane packing density, π_M, determines the lipid−water partition coefficient, K_{lw}, as well as the concentration of half-maximum Pgp activation, K_1, whereby the former decreases (cf. eq 11) and the latter increases (cf. eq 5 and Table 2) with increasing membrane packing density, π_M. The mole fraction of drugs in the membrane, $X_{b(1)}$, that elicits half-maximum Pgp activation is the product of the concentration of half-maximum activation, K_1, and the lipid−water partition coefficient, K_{lw} (*11*),

$$X_{b(1)} = K_1 K_{lw} \tag{20}$$

and is thus *independent* of the membrane packing density, π_M, as illustrated in Table 2 (last column). The mole fraction of the different drugs in the membrane was estimated to be in the range of $X_{b(1)} =$ (0.02 to 67) mmol/mol lipid (cf. Table 1). If we assume that 1 mol of lipid corresponds approximately to 1 L of lipid, the membrane concentration corresponds to about $C_{b(1)} =$ (0.02 to 67) mmol/L lipid.

The high drug concentration in the membrane at half-maximum Pgp activation suggests relatively weak substrate−Pgp interactions. Similarly weak interactions have also been observed for transporters that bind their substrates in the aqueous phase at one side of the membrane and transport them to the aqueous phase at the other side of the membrane, such as the fucose transporter which exhibits a dissociation constant in the mM concentration range (*12*).

The membrane concentration for half-maximum inhibition ($X_{b(2)} = K_2 K_{lw}$) is even higher than that for half-maximum activation, $X_{b(1)}$. For small molecules (e.g. promazine) the mole fraction ratio is small ($X_{b(2)}/X_{b(1)} \approx 2$), and for large molecules (e.g. diltiazem, verapamil, cyclosporin A) the mole fraction ratio is large ($X_{b(2)}/X_{b(1)} \approx 80$), indicating that the accommodation of a second large molecule is more difficult.

The Free Energy of Drug-Binding from the Lipid Membrane to the Activating Binding Region of Pgp, $\Delta G°_{tl(1)}$. The free energy of drug binding from water to activating binding region of Pgp, $\Delta G°_{tw(1)}$, can be expressed as the sum of the free energy of drug partitioning into the lipid membrane, $\Delta G°_{lw}$, and the free energy of drug binding from the lipid phase to the activating binding region of Pgp, $\Delta G°_{tl(1)}$ (cf. eq 6). Figure 5A displays a comparison of $\Delta G°_{tw(1)} = (-30$ to $-54)$ kJ/mol (hatched plus crosshatched), the free energy of drug binding from water to the transporter, with $\Delta G°_{lw} = (-23$ to $-34)$ kJ/mol (crosshatched), the free energy of drug partitioning into the lipid membrane, and $\Delta G°_{tl(1)} = (-7$ to $-27)$ kJ/mol (hatched), the free energy of drug binding from the lipid membrane to the transporter determined for NIH-MDR-G185 cells. For the 15 drugs investigated, $\Delta G°_{lw}$, the free energy of drug partitioning into the lipid membrane, is generally somewhat larger than $\Delta G°_{tl(1)}$, the free energy of drug binding to the activating binding region of the transporter in the lipid phase. However, the variation in $\Delta G°_{tl(1)}$ is more pronounced (∼factor of 4.0) than the variation in $\Delta G°_{lw}$ (∼factor of 1.5).

Figure 5B displays the free energy of drug binding from water, $\Delta G°_{tw(2)} = (-23$ to $-44)$ kJ/mol (hatched plus crosshatched), and from the lipid membrane, $\Delta G°_{tl(2)} = (-1.6$ to $-16)$ kJ/mol (hatched), to the inhibitory binding region of Pgp. The values of $\Delta G°_{lw}$ (crosshatched) are identical to those in Figures 5A and 5B. The free energy of drug binding from water, $\Delta G°_{tw(2)}$, and from the lipid membrane, $\Delta G°_{tl(2)}$, to the inhibitory region of Pgp are thus less negative than the free energies of drug binding to the activating region of Pgp, $\Delta G°_{tw(1)}$ and $\Delta G°_{tl(1)}$.

Kinetic Models and Their Influence on the Estimated Free Energy of Binding to the Transporter. The kinetic data shown in Table 1 were evaluated using the rate eq 2 proposed by Litman et al. (*14*). It is based on the concept of uncompetitive inhibition (or substrate inhibition) which was extended to allow for basal activation in the absence of a substrate and for breakdown of the complex $T(ATP)S_tS_t$ (eq 1). For comparison we fitted our data to a simpler version of uncompetitive inhibition, assuming that the complex $T(ATP)S_tS_t$ (eq 1) is catalytically inactive ($V_2 = 0$) (rate eq 3). While the concentrations of half-maximum activation, K_1, obtained with the two models were similar, the concentrations of half-maximum inhibition, K_2, calculated with the latter model were generally higher. As a consequence the corresponding free energies of binding to the inhibitory binding region of Pgp, $\Delta G°_{tl(2)}$, were less negative (by maximally 15%). The model proposed by Al-Shawi et al. (*33*, *34*) also considers basal activation of Pgp in the absence of drugs, drug activation, and drug inhibition, however, it is based on the concept of noncompetitive inhibition (rate eq 4). Rate eq 4 differs from rate eq 3 only by an additional term, $K_1 C_{sw}$, in the denominator which is small in comparison to the other terms. The free energies of binding, $\Delta G°_{tl(2)}$, obtained with the model of Al-Shawi et al. (*33*, *34*) were therefore similar to those obtained with rate eq 3. The fits to all three models were of comparable quality.

Concentrations of half-maximum activation evaluated by means of a simple Michaelis−Menten equation, K_m (*43*), are generally smaller compared to those obtained with eqs 2−4 (by almost a factor of 2). In terms of free energies of binding, $\Delta G°_{tl(1)}$, the difference is, however, small.

The Nature of Drug−Transporter Interactions. The free energy of drug binding from water to the transporter, $\Delta G°_{tw(1)}$, was shown to be the sum of the free energy of drug partitioning into the lipid membrane, $\Delta G°_{lw}$, and the free energy of drug binding from the lipid phase to the activating binding region of Pgp, $\Delta G°_{tl(1)}$. The interactions which are relevant for binding of a drug from water to the transporter are thus the sum of all the interactions relevant for the two individual binding steps. Drug partitioning into the lipid membrane is dominated by hydrophobic and van der Waals interactions, respectively, with a potential contribution of electrostatic interactions (cf. Figure 4A). The possible nature of the substrate−transporter interactions within the lipid membrane will be discussed in the following. We have shown that the free energy of substrate binding to the transporter within the lipid membrane, $\Delta G°_{tl(1)}$, correlates with the cross-sectional area of the drug, A_D (cf. eq 19 and Figure 6A). However, substrate−transporter interactions are most likely not determined by the size of the substrate as such, but rather by a concomitant increase in residues which can undergo specific interactions with the amino acids in the *transmembrane* sequences of Pgp. Interactions which could play a role are electrostatic (ion−ion or dipole−dipole), hydrogen bonding (weak dipole−dipole), cation−π, π−π

stacking, and van der Waals interactions, respectively, listed in the order of decreasing free energy of binding. The X-ray structure of the multidrug transporter AcrB (at the resolution of (3.5 to 3.8) Å), crystallized with four different drugs bound (in the absence of lipids), suggested the presence of all the different interactions mentioned above (*49*). It has, however, to be considered that the energetic contributions of the diverse interactions differ. Moreover, it has to be considered that not all compounds which bind to Pgp are charged, or carry π-electron systems, but that all of them seem to carry at least one hydrogen bond acceptor pattern (i.e. two hydrogen bond acceptor groups in a distance of 2.5 Å or 4.6 Å) (*23*). Since the free energy contribution of hydrogen bond formation in a hydrophobic environment can be substantial (for review see ref *50*), hydrogen bonding is likely to contribute significantly to the energetics of drug transporter interactions. Hydrogen bond acceptor patterns were therefore suggested to serve as binding modules interacting with the hydrogen bond donor-rich transmembrane domains of Pgp. As a consequence the total free energy of binding of a drug from the lipid membrane to the transporter, $\Delta G^\circ_{tl(1)}$, can be assumed to be the sum of the free energies, ΔG°_{Hi}, of the individual hydrogen bonds formed (*11*, *22*−*24*),

$$\Delta G^\circ_{tl(1)} \approx \sum_{i=1}^{n} \Delta G^\circ_{Hi} = \sum_{i=1}^{n} \Delta H^\circ_{Hi} - T\Delta S^\circ \qquad (21)$$

where ΔH°_{Hi} is the enthalpy change for hydrogen bond formation and $T\Delta S^\circ$ the product of the entropy change upon drug binding and the absolute temperature.

To test whether the assumption made in eq 21 is energetically sound we estimated the free energy per potential hydrogen bond formed, ΔG°_{Hi}, and compared it with literature values. Figure 6B shows the free energy of substrate binding from the lipid membrane to the transporter, $\Delta G^\circ_{tl(1)}$, as a function of the number of weighted hydrogen bond acceptor groups per drug. Since not all hydrogen bond acceptor groups will form hydrogen bonds with the same free energy, we arbitrarily divided them into three groups containing strong (oxygen atoms), intermediate (nitrogen and sulfur atoms as well as phenyl groups), and weak (fluorine atoms) hydrogen bond acceptors, weighted as 1, 0.5, and 0.25, respectively. The average free energy per hydrogen bond, ΔG°_{Hi}, was then estimated by dividing the total free energy of binding, $\Delta G^\circ_{tl(1)}$, by the weighted number of hydrogen bond acceptor groups per drug. The most negative free energy of binding per hydrogen bond, $\Delta G^\circ_{Hi} = -7.8$ kJ/mol, was observed for dibucaine (see Table 1), which exhibits one hydrogen bond acceptor pattern only (corresponding to two hydrogen bonds). For compounds with more than one hydrogen bond acceptor pattern the apparent free energy per hydrogen bond, ΔG°_{Hi}, was less negative. For compounds with more than four hydrogen bond acceptor pattern the apparent free energy per hydrogen bond, ΔG°_{Hi}, reached a limiting value ($\Delta G^\circ_{Hi} \sim -2.5$ kJ/mol). The decrease in ΔG°_{Hi} with increasing number of hydrogen bond acceptors can be explained by a loss in residual motion after formation of more than one hydrogen bond leading to an entropy decrease (*51*). If appropriate membrane packing densities, π_M, are taken into account, comparable values of ΔG°_{Hi} are also obtained from other investigations (e.g. ref *14*). A similar conclusion was drawn previously for undefined binding modules (*25*). The free energy of the first single hydrogen bond formed is therefore most likely $\Delta G^\circ_{Hi} \geq -7.8$ kJ/mol. This value is larger than the free energy estimated for forming an amide hydrogen bond in water ($\Delta G \sim -4$ kJ/mol) and somewhat smaller than the free energy of forming a single hydrogen bond in alkane, determined as $\Delta G \sim -20$ kJ/mol without taking into account entropic effects (*52*). Considering the fact that different types of hydrogen bond acceptors are taken into account, and that possible steric effects are neglected, the resulting free energy value per hydrogen bond seems reasonable and supports the assumption of the modular binding concept proposed previously (eq 21).

The free energy of binding to the inhibitory binding region, $\Delta G^\circ_{tl(2)}$, is on average less negative than that for the activating binding region, $\Delta G^\circ_{tl(1)}$. Nevertheless, it can be assumed that the same type of interactions between drugs and Pgp take place. The less negative free energy of binding, $\Delta G^\circ_{tl(2)}$, is most likely due to conformational changes of the protein upon accommodation of a second molecule which may lead to a decrease in entropy. This is supported by the fact that the difference in free energy, $\Delta G^\circ_{tl(1)} - \Delta G^\circ_{tl(2)}$, increases with increasing the cross-sectional area, A_D, of the drug as seen in Figure 6C. This shows again that accommodation of a large molecule at the inhibitory binding region of Pgp is less favorable than accommodation a small molecule.

Conclusions. Binding of a drug from water to the activating binding region of Pgp occurs in two steps, a partitioning step from water to the lipid membrane, characterized by a lipid−water partition coefficient, K_{lw}, and a binding step from the lipid membrane to the transporter, characterized by a binding constant, $K_{tl(1)}$. The binding constant of a drug from water to the transporter, $K_{tw(1)}$, can thus be expressed as product of two individual binding constants K_{lw} and $K_{tl(1)}$, and the free energy of binding, $\Delta G^\circ_{tw(1)}$, as sum of two corresponding free energies, ΔG°_{lw} and $\Delta G^\circ_{tl(1)}$. The free energies $\Delta G^\circ_{tw(1)}$ and ΔG°_{lw} can be determined independently, which allows estimation of the free energy of binding from lipid to the transporter, $\Delta G^\circ_{tl(1)}$. For the 15 drugs investigated the free energy of drug partitioning into the lipid membrane, ΔG°_{lw}, was generally somewhat more negative than the free energy of drug binding to the transporter in the lipid phase, $\Delta G^\circ_{tl(1)}$. However, the variation in $\Delta G^\circ_{tl(1)}$ was more pronounced (∼factor of 4.0) than the variation in ΔG°_{lw} (less than a factor of 1.5). Drug affinity to the transporter in the lipid membrane was shown to increase with the cross-sectional area, A_D, of the drug. With increasing size of a drug the possibility for different types of interactions also increases. The present analysis suggests that hydrogen bond formation contributes significantly to the energetics of substrate−Pgp interactions within the lipid membrane. Data can be well explained with a modular binding concept, where the binding module in drugs consists of two hydrogen bond acceptor groups. Binding of a drug to Pgp (e.g. hydrogen bond formation) was assumed to be independent of the membrane packing density, π_M, to a first approximation. The mole fraction of drugs, $X_{b(1)}$, in the membrane at the concentration of half-maximum Pgp activation is thus constant, which implies that higher aqueous drug concentrations are required for membrane penetration and Pgp activation in the case of densely packed membranes (e.g.

membranes of *E. coli* bacteria) than in the case of more loosely packed membranes (e.g. mouse embryo fibroblasts). Since the lipid membrane acts as a drug scavenger and interacts synergistically with Pgp, cells are well protected from intruding substrates despite the relatively weak Pgp−substrate interactions.

REFERENCES

1. Dey, S., Ramachandra, M., Pastan, I., Gottesman, M. M., and Ambudkar, S. V. (1997) Evidence for two nonidentical drug-interaction sites in the human P-glycoprotein, *Proc. Natl. Acad. Sci. U.S.A. 94*, 10594−10599.
2. Raviv, Y., Pollard, H. B., Bruggemann, E. P., Pastan, I., and Gottesman, M. M. (1990) Photosensitized labeling of a functional multidrug transporter in living drug-resistant tumor cells, *J. Biol. Chem. 265*, 3975−3980.
3. Chen, Y., Pant, A. C., and Simon, S. M. (2001) P-glycoprotein does not reduce substrate concentration from the extracellular leaflet of the plasma membrane in living cells, *Cancer Res. 61*, 7763−7769.
4. Shapiro, A. B., and Ling, V. (1997) Extraction of Hoechst 33342 from the cytoplasmic leaflet of the plasma membrane by P-glycoprotein, *Eur. J. Biochem. 250*, 122−129.
5. Shapiro, A. B., and Ling, V. (1998) Transport of LDS-751 from the cytoplasmic leaflet of the plasma membrane by the rhodamine-123-selective site of P-glycoprotein, *Eur. J. Biochem. 254*, 181−188.
6. Schmid, D., Ecker, G., Kopp, S., Hitzler, M., and Chiba, P. (1999) Structure−activity relationship studies of propafenone analogs based on P-glycoprotein ATPase activity measurements, *Biochem. Pharmacol. 58*, 1447−1456.
7. Lu, P., Liu, R., and Sharom, F. J. (2001) Drug transport by reconstituted P-glycoprotein in proteoliposomes. Effect of substrates and modulators, and dependence on bilayer phase state, *Eur. J. Biochem. 268*, 1687−1697.
8. Litman, T., Druley, T. E., Stein, W. D., and Bates, S. E. (2001) From MDR to MXR: new understanding of multidrug resistance systems, their properties and clinical significance, *Cell. Mol. Life Sci. 58*, 931−959.
9. Higgins, C. F., and Gottesman, M. M. (1992) Is the multidrug transporter a flippase?, *Trends Biochem. Sci. 17*, 18−21.
10. Seelig, A., Landwojtowicz, E., Fischer, H., and Li Blatter, X. (2003) in *Drug BioAvailability/Estimation of Solubility, Permeability and Absorption* (Van de Waterbeemd, H., Lennernäs, H., Artursson, P. Eds.) pp 461−492, Wiley-VCH Verlag GmbH, Weinheim.
11. Seelig, A., and Gatlik-Landwojtowicz, E. (2005) Inhibitors of multidrug efflux transporters: their membrane and protein interactions, *Mini-Rev. Med. Chem. 5*, 135−151.
12. Spooner, P. J., O'Reilly, W. J., Homans, S. W., Rutherford, N. G., Henderson, P. J., and Watts, A. (1998) Weak substrate binding to transport proteins studied by NMR, *Biophys. J. 75*, 2794−2800.
13. Romsicki, Y., and Sharom, F. J. (1999) The membrane lipid environment modulates drug interactions with the P− glycoprotein multidrug transporter, *Biochemistry 38*, 6887−6896.
14. Litman, T., Zeuthen, T., Skovsgaard, T., and Stein, W. D. (1997) Structure−activity relationships of P-glycoprotein interacting drugs: kinetic characterization of their effects on ATPase activity, *Biochim. Biophys. Acta 1361*, 159−168.
15. Seelig, A., and Landwojtowicz, E. (2000) Structure-activity relationship of P-glycoprotein substrates and modifiers, *Eur. J. Pharm. Sci. 12*, 31−40.
16. Garrigos, M., Mir, L. M., and Orlowski, S. (1997) Competitive and non-competitive inhibition of the multidrug-resistance-associated P-glycoprotein ATPase-further experimental evidence for a multisite model, *Eur. J. Biochem. 244*, 664−673.
17. Landwojtowicz, E., Nervi, P., and Seelig, A. (2002) Real-time monitoring of P-glycoprotein activation in living cells, *Biochemistry 41*, 8050−8057.
18. Gatlik-Landwojtowicz, E., Aanismaa, P., and Seelig, A. (2004) The rate of P-glycoprotein activation depends on the metabolic state of the cell, *Biochemistry 43*, 14840−14851.
19. Shapiro, A. B., Fox, K., Lam, P., and Ling, V. (1999) Stimulation of P-glycoprotein-mediated drug transport by prazosin and progesterone. Evidence for a third drug-binding site, *Eur. J. Biochem. 259*, 841−850.
20. Martin, C., Berridge, G., Higgins, C. F., Mistry, P., Charlton, P., and Callaghan, R. (2000) Communication between multiple drug binding sites on P-glycoprotein, *Mol. Pharmacol. 58*, 624−632.
21. Scala, S., Akhmed, N., Rao, U. S., Paull, K., Lan, L. B., Dickstein, B., Lee, J. S., Elgemeie, G. H., Stein, W. D., and Bates, S. E. (1997) P-glycoprotein substrates and antagonists cluster into two distinct groups, *Mol. Pharmacol. 51*, 1024−1033.
22. Seelig, A., Blatter, X. L., and Wohnsland, F. (2000) Substrate recognition by P-glycoprotein and the multidrug resistance-associated protein MRP1: a comparison, *Int. J. Clin. Pharmacol. Ther. 38*, 111−121.
23. Seelig, A. (1998) A general pattern for substrate recognition by P-glycoprotein, *Eur. J. Biochem. 251*, 252−261.
24. Ecker, G., Huber, M., Schmid, D., and Chiba, P. (1999) The importance of a nitrogen atom in modulators of multidrug resistance, *Mol. Pharmacol. 56*, 791−796.
25. Sauna, Z. E., Andrus, M. B., Turner, T. M., and Ambudkar, S. V. (2004) Biochemical basis of polyvalency as a strategy for enhancing the efficacy of P-glycoprotein (ABCB1) modulators: stipiamide homodimers separated with defined-length spacers reverse drug efflux with greater efficacy, *Biochemistry 43*, 2262−2271.
26. Pajeva, I. K., and Wiese, M. (2002) Pharmacophore model of drugs involved in P-glycoprotein multidrug resistance: explanation of structural variety (hypothesis), *J. Med. Chem. 45*, 5671−5686.
27. Stouch, T. R., and Gudmundsson, O. (2002) Progress in understanding the structure−activity relationships of P-glycoprotein, *Adv. Drug Delivery Rev. 54*, 315−328.
28. Cianchetta, G., Singleton, R. W., Zhang, M., Wildgoose, M., Giesing, D., Fravolini, A., Cruciani, G., and Vaz, R. J. (2005) A pharmacophore hypothesis for P-glycoprotein substrate recognition using GRIND-based 3D-QSAR, *J. Med. Chem. 48*, 2927−2935.
29. McConnell, H. M., Owicki, J. C., Parce, J. W., Miller, D. L., Baxter, G. T., Wada, H. G., and Pitchford, S. (1992) The cytosensor microphysiometer: biological applications of silicon technology, *Science 257*, 1906−1912.
30. Fischer, H., Gottschlich, R., and Seelig, A. (1998) Blood-brain barrier permeation: molecular parameters governing passive diffusion, *J. Membr. Biol. 165*, 201−211.
31. Gerebtzoff, G., Li-Blatter, X., Fischer, H., Frentzel, A., and Seelig, A. (2004) Halogenation of drugs enhances membrane binding and permeation, *ChemBioChem 5*, 676−684.
32. Ambudkar, S. V., Cardarelli, C. O., Pashinsky, I., and Stein, W. D. (1997) Relation between the turnover number for vinblastine transport and for vinblastine-stimulated ATP hydrolysis by human P-glycoprotein, *J. Biol. Chem. 272*, 21160−21166.
33. Al-Shawi, M. K., Polar, M. K., Omote, H., and Figler, R. A. (2003) Transition state analysis of the coupling of drug transport to ATP hydrolysis by P-glycoprotein, *J. Biol. Chem. 278*, 52629−52640.
34. Omote, H., Figler, R. A., Polar, M. K., and Al-Shawi, M. K. (2004) Improved energy coupling of human P-glycoprotein by the glycine 185 to valine mutation, *Biochemistry 43*, 3917−3928.
35. Boguslavsky, V., Rebecchi, M., Morris, A. J., Jhon, D. Y., Rhee, S. G., and McLaughlin, S. (1994) Effect of monolayer surface pressure on the activities of phosphoinositide-specific phospholipase C-beta 1, -gamma 1, and -delta 1, *Biochemistry 33*, 3032−3037.
36. Litman, T., Skovsgaard, T., and Stein, W. D. (2003) Pumping of drugs by P-glycoprotein: a two-step process?, *J. Pharmacol. Exp. Ther. 307*, 846−853.
37. Romani, A. M., and Scarpa, A. (2000) Regulation of cellular magnesium, *Front. Biosci. 5*, D720−D734.
38. Ohki, S., and Kurland, R. (1981) Surface potential of phosphatidylserine monolayers. II. Divalent and monovalent ion binding, *Biochim. Biophys. Acta 645*, 170−176.
39. Seelig, J., Nebel, S., Ganz, P., and Bruns, C. (1993) Electrostatic and nonpolar peptide-membrane interactions. Lipid binding and functional properties of somatostatin analogues of charge $z = +1$ to $z = +3$, *Biochemistry 32*, 9714−9721.
40. Seelig, A. (1987) Local anesthetics and pressure: a comparison of dibucaine binding to lipid monolayers and bilayers, *Biochim. Biophys. Acta 899*, 196−204.
41. Seelig, A., Alt, T., Lotz, S., and Holzemann, G. (1996) Binding of substance P agonists to lipid membranes and to the neurokinin-1 receptor, *Biochemistry 35*, 4365−4374.
42. Blume, A. (1979) A comparative study of the phase transitions of phospholipid bilayers and monolayers, *Biochim. Biophys. Acta 557*, 32−44.

43. Kerr, K. M., Sauna, Z. E., and Ambudkar, S. V. (2001) Correlation between steady-state ATP hydrolysis and vanadate-induced ADP trapping in Human P-glycoprotein. Evidence for ADP release as the rate-limiting step in the catalytic cycle and its modulation by substrates, *J. Biol. Chem. 276*, 8657−8664.
44. Hegner, D. (1980) Age-dependence of molecular and functional changes in biological membrane properties, *Mech. Ageing Dev. 14*, 101−118.
45. Figler, R. A., Omote, H., Nakamoto, R. K., and Al-Shawi, M. K. (2000) Use of chemical chaperones in the yeast Saccharomyces cerevisiae to enhance heterologous membrane protein expression: high-yield expression and purification of human P-glycoprotein, *Arch. Biochem. Biophys. 376*, 34−46.
46. Thurmond, R. L., Dodd, S. W., and Brown, M. F. (1991) Molecular areas of phospholipids as determined by 2H NMR spectroscopy. Comparison of phosphatidylethanolamines and phosphatidylcholines, *Biophys. J. 59*, 108−113.
47. Gally, H. U., Pluschke, G., Overath, P., and Seelig, J. (1979) Structure of Escherichia coli membranes. Phospholipid conformation in model membranes and cells as studied by deuterium magnetic resonance, *Biochemistry 18*, 5605−5610.
48. Nichol, C. P., Davis, J. H., Weeks, G., and Bloom, M. (1980) Quantitative study of the fluidity of Escherichia coli membranes using deuterium magnetic resonance, *Biochemistry 19*, 451−7.
49. Yu, E. W., McDermott, G., Zgurskaya, H. I., Nikaido, H., and Koshland, D. E., Jr. (2003) Structural basis of multiple drug-binding capacity of the AcrB multidrug efflux pump, *Science 300*, 976−980.
50. Baldwin, R. L. (2005) in *Protein Folding Handbook. Part I* (Kiefhaber, J. B. a. T., Ed.) pp 127−162, Wiley-VCH Verlag GmbH & Co. KGaA, Weinheim.
51. Tobey, S. L., and Anslyn, E. V. (2003) Studies into the thermodynamic origin of negative cooperativity in ion-pairing molecular recognition, *J. Am. Chem. Soc. 125*, 10963−10970.
52. Ben-Tal, N., Sitkoff, D., Topol, I. A., Yang, A.-S., Burt, S. K., and Honig, B. (1997) Free Energy of Amide Hydrogen Bond Formation in Vacuum, in Water, and in Liquid Alkane Solution, *J. Phys. Chem. B 101*, 450−457.
53. Frisk-Holmberg, M., and van der Kleijn, E. (1972) The relationship between the lipophilic nature of tricyclic neuroleptics and antidepressants, and histamine release, *Eur. J. Pharmacol. 18*, 139−147.
54. Clarke, F. H. (1984) Ionization constants by curve fitting: application to the determination of partition coefficients, *J. Pharm. Sci. 73*, 226−230.
55. Tollenaere, J. P. (1977) Conformation of neuroleptic drugs in 3 aggregation states and their conformational resemblance to dopamine, *Eur. J. Med. Chem. 12*, 199−211.
56. Frézard, F., and Garnier-Suillerot, A. (1998) Permeability of lipid bilayer to anthracycline derivatives. Role of the bilayer composition and of the temperature, *Biochim. Biophys. Acta 1389*, 13−22.
57. Ritchie, J. M., and Greengard, P. (1961) On the active structure of local anesthetics, *J. Pharmacol. Exp. Ther. 133*, 241−245.
58. Hwang, K. K., Martin, N. E., Jiang, L., and Zhu, C. (2003) Permeation prediction of M100240 using the parallel artificial membrane permeability assay, *J. Pharm. Pharm. Sci. 6*, 315−320.
59. Tenthorey, P. A., Block, A. J., Ronfeld, R. A., McMaster, P. D., and Byrnes, E. W. (1981) New antiarrhythmic agents. 6. Quantitative structure-activity relationships of aminoxylidides, *J. Med. Chem. 24*, 798−806.
60. Seiler, P. (1974) Interconversion of lipophilicities from hydrocarbon-water systems into octanol-water system, *Eur. J. Med. Chem. 9*, 473−479.
61. Hasegawa, J., Fujita, T., Hayashi, Y., Iwamoto, K., and Watanabe, J. (1984) pKa determination of verapamil by liquid-liquid partition, *J. Pharm. Sci. 73*, 442−445.
62. Budavari, S. (1996), Merck Research Laboratories Division of Merck & Co., Inc., New Jersey.
63. Clarke, F. H., and Cahoon, N. M. (1987) Ionization constants by curve fitting: determination of partition and distribution coefficients of acids and bases and their ions, *J. Pharm. Sci. 76*, 611−620.
64. Franke, U., Munk, A., and Wiese, M. (1999) Ionization constants and distribution coefficients of phenothiazines and calcium channel antagonists determined by a pH-metric method and correlation with calculated partition coefficients, *J. Pharm. Sci. 88*, 89−95.

BI051380+